Extremely large magnetoresistance and Shubnikov–de Haas oscillations in the compensated semimetal W_2As_3

Lingxiao Zhao,[1,2,3] Junbao He,[2,3] Dong Chen,[2,3] Shuai Zhang,[2] Zhian Ren,[2,3] and Genfu Chen[2,3,*]

[1]*Wuhan National High Magnetic Field Center School of Physics, Huazhong University of Science and Technology, Wuhan 430074, China*

[2]*Institute of Physics and Beijing National Laboratory for Condensed Matter Physics, Chinese Academy of Sciences, Beijing 100190, China*

[3]*School of Physical Sciences, University of Chinese Academy of Sciences, Beijing 100190, China*

(Received 25 September 2018; revised manuscript received 5 April 2019; published 10 May 2019)

We report the extremely large magnetoresistance (XMR) property and Shubnikov–de Haas (SdH) oscillations in a quasi-one-dimensional material W_2As_3 single crystal, which shows good metallic behavior with a typical residual resistivity ratio $\rho(300\ \mathrm{K})/\rho(1.8\ \mathrm{K}) = 1240$. In a magnetic field, the resistivity shows a quick upturn behavior and saturates with a plateau as the temperature cools down. At $T = 1.8$ K, the magnetoresistance of W_2As_3 increases quadratically with the magnitude of the magnetic field and reaches up to 32 000% ($B = 9$ T) without any trend of saturation, which suggests the semiclassical nature during the transport process. The result of Hall resistivity measurements further points out that the XMR property in W_2As_3 originates from the compensation of electrons and holes with high mobility ($\mu_e = 4.9 \times 10^4\ \mathrm{cm^2\ V^{-1}\ s^{-1}}$ at 1.8 K). Furthermore, SdH oscillations can be distinguished clearly from both magnetoresistivity and Hall resistivity. The quantum mobility calculated from the SdH oscillations is about 1–2 orders lower than that calculated from the transport mobility, which suggests that the small angle scattering is dominant in W_2As_3. The angle dependence of SdH oscillations implies the complex Fermi surface structure with obvious anisotropy in W_2As_3.

DOI: 10.1103/PhysRevB.99.205116

I. INTRODUCTION

Searching for new materials with large magnetoresistance (MR) is an interesting research topic since the discovery of the giant-magnetoresistance (GMR) property in the magnetic system, which is later widely used as information storage material. Recently, the discovery of the extremely large magnetoresistance (XMR) phenomenon in WTe_2 [1] has renewed the research interest on searching for materials with large MR especially in the nonmagnetic semimetals. From then on, researchers have studied and discovered a series of nonmagnetic materials with XMR property [2–16]. Till now, two main mechanisms have arguably obtained attention to explain the XMR effect in those nonmagnetic semimetals. One is the topological protection. In topological materials, the backscattering is suppressed by the topological protection without magnetic field [17,18]. The lifting of this protection by an external magnetic field leads to the XMR [2]. Topologically nontrivial electronic structure with linear band dispersion is the key factor in this condition. Several materials have been confirmed to be the topological semimetals, such as Cd_3As_2 [19], TaAs family [20,21], $PtSn_4$ [22], ZrSiS [23], etc. The other one is the electron-hole compensation scenario. Under the perfect e-h "resonance" condition, the MR increases quadratically with the strength of magnetic field B without any sign of saturation. For example, α-As [7], $PtBi_2$ [8], $TaAs_2$ [9], YSb [10], and $NbSb_2$ [11] were found to be the good compensated semimetals with MR over 10^5%. Recently, W_2As_3 was reported as a new compensated semimetal with XMR property by Li *et al.* [24]. Topological features and multiband features were proposed by them via the first-principles calculations and the quantum oscillations analysis.

At the same time, we successfully grew high quality W_2As_3 single crystals and studied the transport properties independently. We found the XMR property in it and analyzed the SdH oscillations in detail. Especially, we discovered obvious anisotropy from both magnetoresistance and FFT frequencies of the SdH oscillations in this quasi-one-dimensional material. The MR ($\mathrm{MR}(B) = [\rho(B) - \rho(0)]/\rho(0)$) of our sample reaches 32 000% in 1.8 K and 9 T without any sign of saturation. The result of Hall resistivity measurements further points out that the XMR property in W_2As_3 is attributed to the compensation of electrons and holes with high mobility. Analysis of the SdH oscillations observed in W_2As_3 indicates the existence of several relatively small Fermi pockets occupied in the first Brillouin zone. The extremely low Dingle temperature supports the high quality of our sample. Furthermore, we found that the quantum mobilities calculated from the SdH oscillations are about 1–2 orders lower than that calculated from the transport mobility, which suggests that the small angle scattering is dominant in W_2As_3. The angle dependence of SdH oscillations implies the complex Fermi surface structure with obvious anisotropy in W_2As_3.

II. EXPERIMENT

High quality single crystals of W_2As_3 were grown by the chemical vapor transport (CVT) method using Br_2 as the transport agent. First, W_2As_3 predecessors were pre-sintered

*gfchen@iphy.ac.cn

by solid state reaction using high purity powder of W (99.9%) and As (99.9999%) in an evacuated quartz tube. Then the products were reground and sealed in an evacuated quartz tube with Br_2 and were transformed into a two-zone furnace. A temperature gradient from 950 °C (source) to 800 °C (sink) was used during the crystal growth. After one month, needlelike single crystals were obtained at the hot end of the tube. The obtained crystals were characterized by x-ray diffraction (XRD) recorded by a PANalytical diffractometer with Cu k_α radiation ($\lambda = 1.5406$ Å). The atomic proportion examined by energy dispersive x-ray (EDX) spectroscopy was consistent with 2:3 for W:As (not shown here). The magnetoresistivity and Hall effect measurements were performed in a physical property measurement system (Quantum Design PPMS-9) with a temperature range from 1.8 to 300 K. The SdH oscillations in W_2As_3 was carefully measured on a TeslatronPT (Oxford Instruments) equipped with a homemade rotator whose angle can be controlled by a data-collecting computer. The electrical current was applied by a Keithley 6221 and the voltage was measured by a Keithley 2182A. The magnetic field was perpendicular to the current during the rotation.

III. RESULTS

The crystal structure of W_2As_3 [25] was reported to be a monoclinic structure with the space group of $C12/m1$. The refined lattice parameters are $a = 13.372$ Å, $b = 3.279$ Å, $c = 9.599$ Å, $\alpha = 90°$, $\beta = 124.592°$, and $\gamma = 90°$. Figure 1(a) shows the crystal structure of W_2As_3, where the b axis is perpendicular to the ac plane. The inset of Fig. 1(b) shows the image of an as-grown W_2As_3 single crystal with the size of $4.5 \times 0.2 \times 0.05$ mm^3. Figure 1(b) is the XRD pattern of the W_2As_3 single crystal. Only the set of (h 0 0) showed up, indicating the facet of the sample shown in the inset of Fig. 1(b) is the bc plane. Additionally, we confirmed that the long edge of the sample is along the b axis, which was labeled with the blue arrow in the inset of Fig. 1(b). (For the method see Ref. [26], the result is not shown here.) During all of our measurements, the current was kept along the b axis. Figure 1(c) shows the temperature dependence of resistivity under various magnetic fields. At $B = 0$ T, W_2As_3 sample exhibits a perfect metallic behavior with the residual resistivity ratio RRR $= \rho(300\ \text{K})/\rho(1.8\ \text{K}) = 1240$. The quite high RRR indicates the high sample quality which can better reflect the inherent property of W_2As_3. When the magnetic field is applied, the resistivity shows a quick upturn behavior and saturates with a plateau as the temperature cools down. In other words, with temperature decreasing, the resistivity reduces to the minimum at T_m, then increases rapidly with an inflection at T_i and finally saturates with a resistivity plateau. Similar behaviors have been observed in many semimetals, including the recently discovered topological semimetals, such as WTe_2 [1], TaAs [3], $PtSn_4$ [5], $PtBi_2$ [8], ZrSiS [27], as well as traditional semimetal like graphite [28] and bismuth [29]. These materials share a commonality that their carrier mobilities are always very high (10^4–10^6 cm^2 V^{-1} s^{-1}) at low temperatures. However, the origin of the field-induced resistivity upturn is still under debate. To get a more clear view of the exotic transport behavior, we plot several $\partial\rho_{xx}/\partial T$ curves under different temperatures shown in Fig. 1(d), where

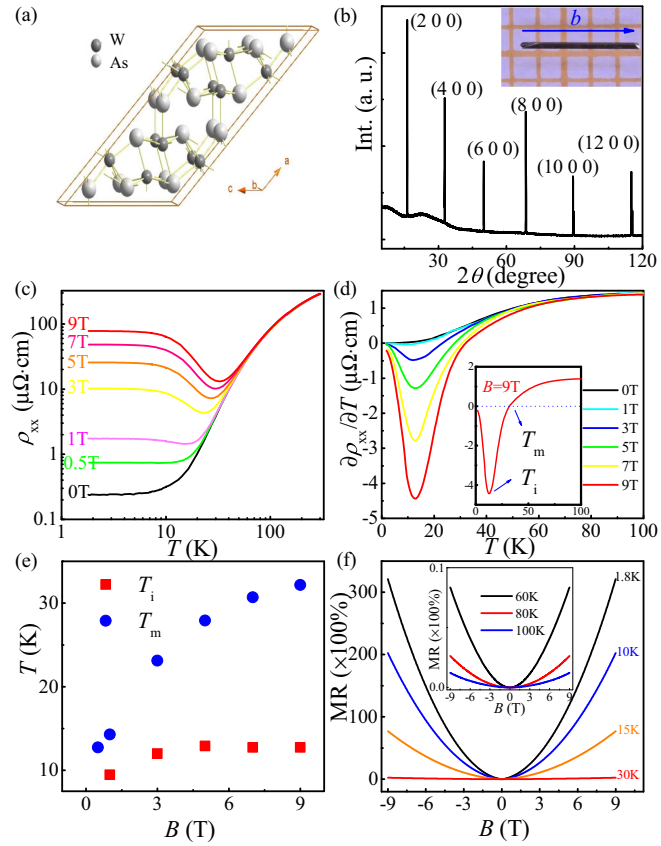

FIG. 1. (a) Crystal structure of W_2As_3. (b) X-ray diffraction pattern of W_2As_3 single crystal, showing only the (h 0 0) reflection. Inset: Picture of a W_2As_3 single crystal with the typical size of $4.5 \times 0.2 \times 0.05$ mm^3. (c) Temperature dependence of the resistivity under different magnetic field ($B = 0$, 0.5, 1, 3, 5, 7, and 9 T) on log-log scale. (d) The derivative curves taken under different magnetic fields. Inset shows the crossover temperature (T_m) and plateau temperature (T_i) for $B = 9$ T. (e) T_m and T_i vs magnetic field. (f) Magnetic field dependence of MR at various temperatures when the magnetic field is perpendicular to the current.

the T_m and T_i are denoted by the temperatures at which $\partial\rho_{xx}/\partial T$ curves change sign and take a minimum, as plotted in the inset of Fig. 1(d). Then we plot the phase diagram of T_i and T_m as a function of B in Fig. 1(e), showing that T_m changes slowly but T_i increases rapidly with the magnetic field increasing. Figure 1(f) shows the magnetic field dependence of MR at various temperatures for the field perpendicular to the current. The MR increases quadratically with the magnetic field rising and finally approaches 3.2×10^4% at $T = 1.8$ K under the magnetic field of 9 T without any sign of saturation. Furthermore, we measured the MR under the magnetic field up to 14 T and $T = 1.5$ K, the MR keeps the quasisquared behavior and reaches 6.9×10^4% (see the Supplemental Material [30]). According to the semiclassical theory, the MR can be expressed as the following equation [7]:

$$\text{MR} = \frac{(n_h\mu_h - n_e\mu_e)^2(1 + \mu_h\mu_e B^2)}{(n_h\mu_h - n_e\mu_e)^2 + B^2\mu_h^2\mu_e^2(n_h + n_e)^2}, \qquad (1)$$

where n_e (n_h) is the carrier density of the electron (hole), and μ_e (μ_h) is the mobility of the electron (hole), respectively.

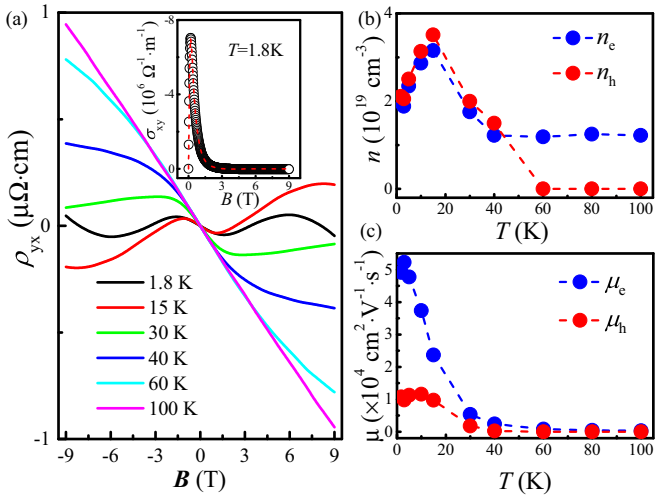

FIG. 2. (a) Hall resistivity of W_2As_3 measured at various temperatures from 1.8 to 100 K. Inset: Magnetic field dependence of σ_{xy} at various temperatures. The open circles and the dotted lines represent the measured data and the fitting result with the two-carrier mode, respectively. (b) Temperature dependence of carrier densities n_h and n_e. (c) Temperature dependence of carrier mobility μ_h and μ_e for different carriers deduced by the two-carrier model.

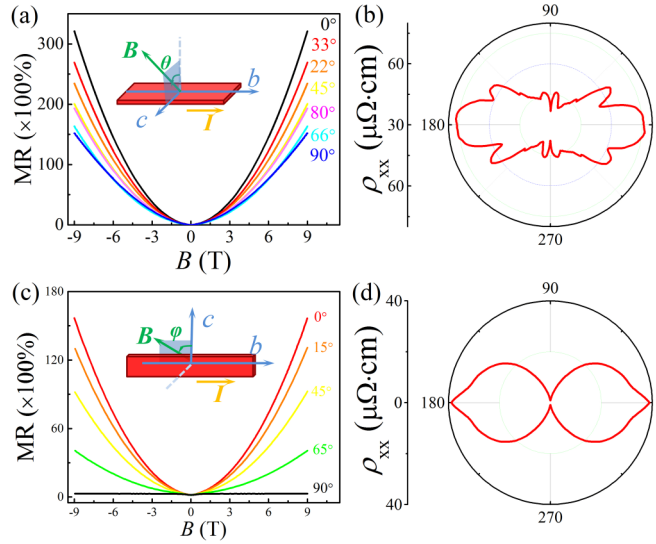

FIG. 3. (a) and (c) MR of W_2As_3 at 1.8 K versus the strength of magnetic field applied at different angles θ and φ, respectively. Inset: The measurement configurations. (b) and (d) The polar plot for the angle dependence of the resistivity under 9 T and 1.8 K, corresponding to (a) and (c), respectively.

In the case of the perfect compensation condition where $n_e = n_h$, the formula can be simplified as $\mathrm{MR} = \mu_e\mu_h B^2$, where the MR increases quadratically with the magnetic field without saturation. Using this formula, we can estimate that the carrier mobility of W_2As_3 is about 10^4 cm^2 V^{-1} s^{-1} at low temperature.

We measured magnetic-field-dependent Hall resistivity of W_2As_3 at different temperatures to further study the carrier densities and mobilities and the results are presented in Fig. 2(a). At low temperatures, the nonlinear feature of ρ_{yx} persists up to the highest applied magnetic fields. Furthermore, both the Hall resistivity and its slope change their signs, revealing the coexistence of electrons and holes in W_2As_3. At higher temperatures, the ρ_{yx}-B curves tend to be linearly dependent especially above 100 K, meaning that the holes play a leading role at high temperature. We fitted the hole and electron densities and mobilities with a simple two-carrier model [3],

$$\sigma_{xy}(B) = \frac{\rho_{yx}(B)}{\rho_{xx}^2(B) + \rho_{yx}^2(B)} = \left[\frac{n_h\mu_h^2}{1+(\mu_h B)^2} - \frac{n_e\mu_e^2}{1+(\mu_e B)^2}\right]eB. \quad (2)$$

Here n_h (n_e) denotes the carrier density of holes and electrons and μ_h (μ_e) denotes the mobility of holes and electrons, respectively. The fitted result of the transverse conductivity is shown in the inset of Fig. 2(a), which yields carrier densities of $n_h = 2.10 \times 10^{19}$ cm^{-3} (hole) and $n_e = 1.98 \times 10^{19}$ cm^{-3} (electron) with corresponding carrier mobilities of $\mu_h = 1.07 \times 10^4$ cm^2 V^{-1} s^{-1} and $\mu_e = 4.92 \times 10^4$ cm^2 V^{-1} s^{-1}, respectively. The excellent agreement between the experimental data and fitted results according to the two-carrier model at 1.8 K confirms the coexistence of electrons and holes in W_2As_3 at low temperature. The good carriers compensation with high mobility in W_2As_3 should be the main reasons which cause the unsaturated quadratic large MR.

In order to investigate the anisotropy of W_2As_3, we measured the angle dependence of the ρ_{xx} by tilting the magnetic field around the b axis and in the bc plane separately in the same single crystal. The results are shown in Fig. 3, in which we used the raw data to ensure the facticity of the result. During the measurements, the current were applied along the b axis, the longest direction of the crystal. The measurement configurations are shown in the inset of Figs. 3(a) and 3(c). In Fig. 3(a) it clearly shows that the MR rises quadratically with the magnetic field increasing, but decreases gradually when tilting the magnetic field from $\theta = 0^\circ$ to $\theta = 90^\circ$. Figure 3(b) shows a polar plot of ρ_{xx} under 9 T and 1.8 K with tilting the magnetic field around the b axis. The resistivity shows a strange behavior with several extreme points with the θ increasing, indicating a complex Fermi surface in W_2As_3. Besides, the scale of MR decreases from 32 000% to 15 000% with the θ increasing from 0° to 90°, indicating a clear anisotropy around the b axis of the Fermi surface. Additionally, we did the measurements by tilting the magnetic field in the bc plane. The sharp angle emerges around $\varphi = 0^\circ$ and decreases significantly with the angle φ increasing. The anisotropic of the magnetoresistence [$\mathrm{MR}(\varphi = 0^\circ)/\mathrm{MR}(\varphi = 90^\circ)$] is about 3700% under this circumstance.

Figures 4(a)–4(d) show the SdH oscillations extracted from the ρ_{xx} when the magnetic field is applied perpendicular to the bc plane. Figure 4(a) presents the oscillation parts against the reciprocal of the magnetic field $1/B$. Figure 4(b) presents the fast Fourier transformation (FFT) spectrum of $\Delta\rho_{xx}$ from 1.8 to 3 K. Five fundamental frequencies $F_\alpha^{bc} = 313$ T, $F_\beta^{bc} = 578$ T, $F_\gamma^{bc} = 653$ T, $F_\delta^{bc} = 1715$ T, and $F_\varepsilon^{bc} = 2032$ T can be identified clearly. According to the Onsager relation $F = (\hbar c/2\pi e)A_k$, the oscillation frequency is proportional to the extreme cross section. We calculated the extremal

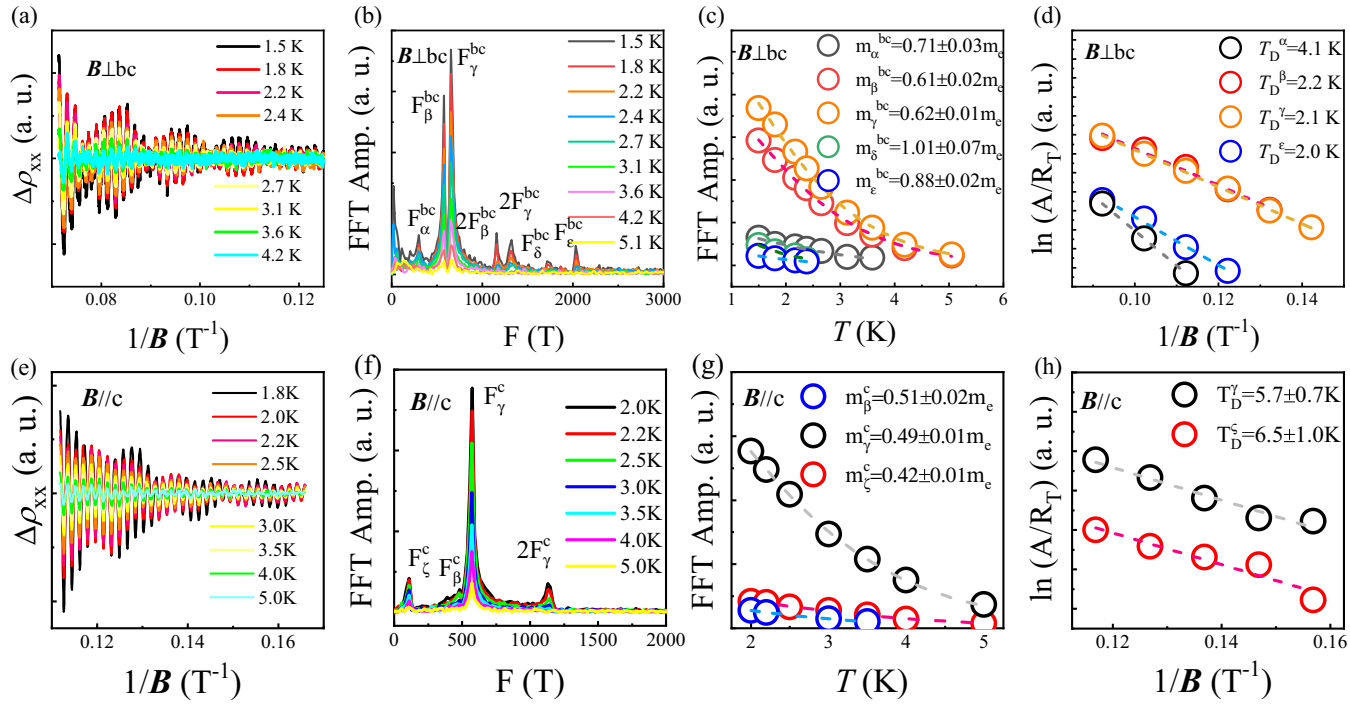

FIG. 4. SdH oscillations of W_2As_3 when $B \perp bc$ plane (a)–(d) and $B \parallel c$ axis (e)–(h). (a) and (e) Residual resistivity extracted from the polynomial fits vs $1/B$ measured at 1.8 K. (b) and (f) The FFT spectrum of $\Delta\rho_{xx}$ at different temperatures. (c) and (g) Temperature dependence of the amplitude for the three frequencies, and the dashed curves are theoretical fittings to the Lifshitz-Kosevitch formula. (d) and (h) Dingle temperatures of different pockets.

Fermi surface areas, which are $S_F^\alpha = 0.030$ Å^{-2}, $S_F^\beta = 0.055$ Å^{-2}, $S_F^\gamma = 0.062$ Å^{-2}, $S_F^\delta = 0.163$ Å^{-2}, and $S_F^\varepsilon = 0.194$ Å^{-2} occupying 2.4%, 4.4%, 5.0%, 13.1%, and 15.5% of the first Brillouin zone, respectively.

With the temperature increasing, the oscillation amplitude damps out gradually. The amplitude can be expressed by the Lifshitz-Kosevitch formula [31] $R_T = \frac{X}{\sinh X}$ and impurity scattering $R_D = \exp(-\frac{\pi m^*}{eB\tau_Q})$, where $X = \frac{2\pi^2 k_B T m^*}{e\hbar B}$, m^* is the cyclotron mass, and T_D is the Dingle temperature. We plot the temperature dependence of the amplitude and the fitted curves for these three frequencies in Fig. 4(c). The fitted cyclotron masses are $m_\alpha^* = (0.71 \pm 0.03)m_e$, $m_\beta^* = (0.61 \pm 0.02)m_e$, $m_\gamma^* = (0.62 \pm 0.01)m_e$, $m_\delta^* = (1.01 \pm 0.07)m_e$, and $m_\varepsilon^* = (0.88 \pm 0.02)m_e$, which are lighter than or approximate to the mass of the free electron. The fitted Dingle temperatures are $T_D^\alpha = 4.1$ K, $T_D^\beta = 2.2$ K, $T_D^\gamma = 2.1$ K, and $T_D^\varepsilon = 2.0$ K for α, β, γ, and ε bands, but we failed to figure out the Dingle temperature of the δ band because of the small oscillation amplitude. These rather low Dingle temperatures indicate small scattering rates, which further supports the high sample quality. Quantum scattering lifetime τ_Q is reciprocal to the Dingle temperature $\tau_Q = \hbar/2\pi k_B T_D$. In this material, $\tau_Q^\alpha = 3.0 \times 10^{-13}$ s, $\tau_Q^\beta = 5.5 \times 10^{-13}$ s, $\tau_Q^\gamma = 5.8 \times 10^{-13}$ s, and $\tau_Q^\varepsilon = 6.1 \times 10^{-13}$ s, longer than that in the topological semimetal $PtBi_2$ [8], which shows very large XMR property (1.12×10^7%) at 1.8 K and 33 T. The carrier mobilities are estimated by $\mu_Q = (e\tau_Q/m^*)$, giving that $\mu_Q^\alpha = 734$ cm^2 V^{-1} s^{-1}, $\mu_Q^\beta = 1593$ cm^2 V^{-1} s^{-1}, $\mu_Q^\gamma = 1642$ cm^2 V^{-1} s^{-1}, and $\mu_Q^\varepsilon = 1214$ cm^2 V^{-1} s^{-1}, which are about one order lower than μ_{tr}. The transport lifetime $\tau_{tr} = \mu m^*/e$ are about 10^{-11} s. The large ratio of τ_{tr}/τ_Q and μ_{tr}/μ_Q suggests that the small angle scattering is dominant in W_2As_3 [32,33].

Additionally, we rotated the crystal by 90° around the b axis and investigated the anisotropy of the Fermi surface of W_2As_3. Results were shown from Fig. 4(e) to Fig. 4(h). Three fundamental frequencies can be clearly identified, which are labeled with F_β^c, F_γ^c, and F_ζ^c according to the angle dependence of the SdH oscillations discussed below. Results are listed in Table I.

We noticed that the frequencies of Shubnikov–de Haas oscillations are quite different between Ref. [24] and our results when $B \perp bc$ plane. There are three possible reasons in our opinion. The first reason is different sample quality which can influence the transport property remarkably. The second reason is related to the inner property of the carriers. According to the Lifshitz-Kosevich formula,

$$\frac{\Delta\rho}{\rho} \propto \frac{2\pi^2 k_B T m^*/eB\hbar}{\sinh(2\pi^2 k_B T m^*/eB\hbar)} \exp(-2\pi^2 k_B T_D m^*/eB\hbar). \quad (3)$$

The amplitude of the oscillations relates to the cyclotron mass (m^*), Dingle temperature (T_D), temperature (T), and the magnetic field (B). The cyclotron mass of the carriers (m_{h1}, m_{h3}, m_{e2}, and m_{h5}) reported in Ref. [24] are similar to F_{e3} (labeled as F_ε in our work). If we believe these carriers really exist, we can conjecture that the Dingle temperature of these pockets are much larger than other pockets so that the amplitude of these oscillations fade out fast with the field decreasing. The last reason is the misalignment of the sample and the magnetic field. In the sample with high anisotropy a little misalignment may cause a significant difference in

TABLE I. Summary of the physical properties: Frequencies (F), exterminal Fermi surface area (S_F), cyclotron mass (m^*), Dingle temperature (T_D), relaxation time (τ_Q), and carrier mobilities (μ_Q) of each pocket when the magnetic field is paralleled or perpendicular to the normal direction of the bc plane.

Pockets	α	β	γ	δ	ε	ζ
F^{bc} (T)	313	578	653	1715	2032	
F^{c} (T)		482	571			111
S_F^{bc} (Å^{-2})	0.030	0.055	0.062	0.163	0.194	
S_F^{c} (Å^{-2})		0.046	0.055			0.011
Fraction^{bc}	2.4%	4.4%	5.0%	13.1%	15.5%	
Fraction^{c}		4.2%	5.0%			1.0%
m_{bc}^* (m_e)	0.71 ± 0.03	0.61 ± 0.02	0.62 ± 0.01	1.01 ± 0.07	0.88 ± 0.02	
m_c^* (m_e)		0.51 ± 0.02	0.49 ± 0.01			0.42 ± 0.01
T_D^{bc} (K)	4.1	2.2	2.1		2.0	
T_D^{c} (K)			5.9			6.5
τ_Q^{bc} (s)	3.0×10^{-13}	5.5×10^{-13}	5.8×10^{-13}		6.1×10^{-13}	
τ_Q^{c} (s)			2.1×10^{-13}			1.9×10^{-13}
μ_Q^{bc} (cm^2/V s)	734	1593	1642		1214	
μ_Q^{c} (cm^2/V s)			760			790

quantum oscillations, for the extreme orbit may emerge or disappear over a special angle.

In order to gain a further insight into the quantum oscillations and anisotropy of W_2As_3, we studied angular dependent magnetoresistance by rotating the sample around the b axis. The current was applied along the b axis and the magnetic field was rotated in the ac plane. The schematic diagram of experimental setup is shown in Fig. 5(a). Figure 5(b) is the shifted FFT spectra of SdH as a function of frequency from 0° to 180°. We picked up the peaks of the FFT spectra and plotted them with the FFT spectra in Fig. 5(c). The frequencies evolve complicatedly with the increasing of angle. The frequencies F_β and F_γ varied continuously from 0° to 180°, but F_α, F_δ, and F_ε disappear quickly when the angle rotted away from 0°. Meanwhile, new frequencies labeled as $F_{\beta'}$, $F_{\beta''}$, F_η, F_ζ, $F_{\zeta'}$, and $F_{\zeta''}$ emerge. These sporadic frequencies indicate a complex Fermi surface in W_2As_3. It is notable that the frequencies $F_{\beta'}$, F_η, F_ζ, $F_{\zeta'}$, and $F_{\zeta''}$ occur when the angle θ just turn a little away from 0°. This result illustrates that the high anisotropy causes significantly different FFT frequencies in W_2As_3.

In order to clarify the symmetry of the Fermi surface, we plotted the angle dependence of fundamental frequencies in a polar plot in Figs. 6(a) and 6(b). It is clear that the frequencies show a twofold rotational symmetry and the γ pocket looks

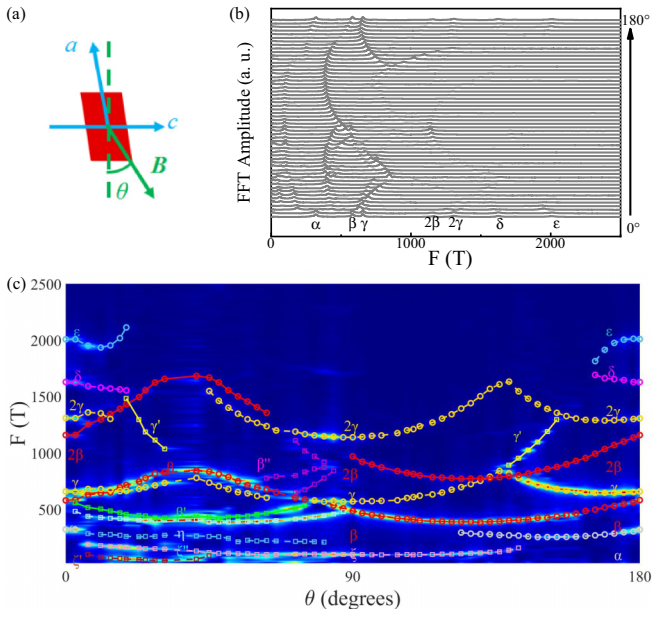

FIG. 5. Angle dependence of the SdH oscillations of W_2As_3. (a) Schematic diagram of the sample geometry for measurement. (b) Shifted FFT spectra of SdH oscillations as a function of frequency from 0° to 180°. (c) Angular dependence of SdH frequencies. The circles are for experimental data from the peaks of the FFT spectra.

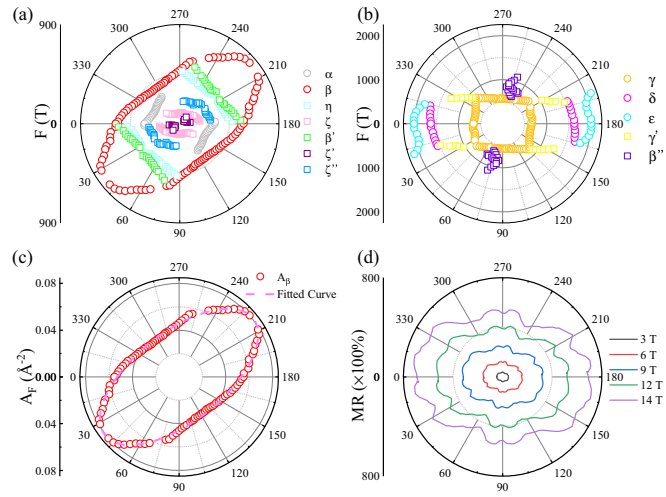

FIG. 6. (a) and (b) The angle dependence of the fundamental frequencies in a polar plot. (c) The angle dependence of the cross section area of the β pocket. (d) The angle dependence of MR measured at 1.5 K.

like a rectangle with quasifourfold symmetry. Besides, the β pocket is like a ellipse. We calculated the angle dependence of the cross section area of the β pocket using the Onsager relation. Then we plotted the angle dependence of A_β and fit it with the formula [10]

$$A_\beta = A_{\beta 0}\sqrt{[\cos(\theta-\varphi)]^2 + [\lambda \sin(\theta-\varphi)]^2}, \qquad (4)$$

where we obtain $A_{\beta 0} = 0.0807$ Å^{-2}, $\lambda = 2.1$, and $\varphi = 38.2^\circ$. It should be noted that the A_F increased to the maximum value at $\theta = 38.2^\circ$ when the magnetic field is around the normal direction of the a axis where the MR exhibit an extremely large point. We can consider that the anisotropy of the MR is affected by the complex Fermi surface with significant anisotropy. Figure 6(d) shows the angle dependence of MR at 1.5 K. The shape of the MR-θ curve almost does not change with the magnetic field up to 14 T. This suggests that the anisotropy of the MR is independent of the value of the magnetic field.

IV. CONCLUSION

In summary, high quality W_2As_3 single crystals have been grown successfully, and large magnetoresistance and field induced resistivity upturn phenomenon are observed. MR approaches 32 000% in 1.8 K, 9 T without saturation. The large MR significantly changes with the magnetic field rotation, indicating an anisotropic electronic structure in W_2As_3. The analysis of Hall effect points out that the XMR property in W_2As_3 can be explained by the carriers compensation scenario. Clear SdH oscillations have been observed and three fundamental frequencies can be clearly identified. Cyclotron mass, Dingle temperature, relaxation time, and carriers mobilities are also estimated through SdH oscillations. Comparing with the transport result, the result suggests that the small angle scattering is dominant in W_2As_3. The angle dependence of SdH oscillations implies the complex Fermi surface structure with obvious anisotropy in W_2As_3.

ACKNOWLEDGMENTS

This work was supported by the National Basic Research Program of China 973 Program (Grant No. 2015CB921303), the National Key Research Program of China (Grant No. 2016YFA0300604), the Strategic Priority Research Program (B) of Chinese Academy of Sciences (Grant No. XDB07020100), the National Natural Science Foundation of China (Grant No. 11874417), and the China Postdoctoral Science Foundation (2018M630846).

[1] M. N. Ali, J. Xiong, S. Flynn, J. Tao, Q. D. Gibson, L. M. Schoop, T. Liang, N. Haldolaarachchige, M. Hirschberger, N. P. Ong, and R. J. Cava, Nature (London) **514**, 205 (2014).
[2] T. Liang, Q. Gibson, M. N. Ali, M. Liu, R. J. Cava, and N. P. Ong, Nat. Mater. **14**, 280 (2014).
[3] X. C. Huang, L. X. Zhao, Y. J. Long, P. P. Wang, D. Chen, Z. H. Yang, H. Liang, M. Q. Xue, H. M. Weng, Z. Fang, X. Dai, and G. F. Chen, Phys. Rev. X **5**, 031023 (2015).
[4] C. Shekhar, A. K. Nayak, Y. Sun, M. Schmidt, M. Nicklas, I. Leermakers, U. Zeitler, Y. Skourski, J. Wosnitza, Z. Liu, Y. Chen, W. Schnelle, H. Borrmann, Y. Grin, C. Felser, and B. Yan, Nat. Phys. **11**, 645 (2015).
[5] N. H. Jo, Y. Wu, L. L. Wang, P. P. Orth, S. S. Downing, S. Manni, D. Mou, D. D. Johnson, A. Kaminski, S. L. Bud'ko, and P. C. Canfield, Phys. Rev. B **96**, 165145 (2017).
[6] G. Peramaiyan, R. Sankar, I. P. Muthuselvam, and W. L. Lee, Sci. Rep. **8**, 6414 (2018).
[7] L. X. Zhao, Q. N. Xu, X. M. Wang, J. B. He, J. Li, H. X. Yang, Y. J. Long, D. Chen, H. Liang, C. H. Li, M. Q. Xue, J. Q. Li, Z. Ren, L. Lu, H. M. Weng, Z. Fang, X. Dai, and G. F. Chen, Phys. Rev. B **95**, 115119 (2017).
[8] W. S. Gao, N. N. Hao, F. W. Zheng, W. Ning, M. Wu, X. D. Zhu, G. L. Zheng, J. L. Zhang, J. W. Lu, H. W. Zhang, C. Y. Xi, J. Y. Yang, H. F. Du, P. Zhang, Y. H. Zhang, and M. L. Tian, Phys. Rev. Lett. **118**, 256601 (2017)
[9] Y.-Y. Wang, Q.-H. Yu, P.-J. Guo, K. Liu, and T.-L. Xia, Phys. Rev. B **94**, 041103(R) (2016).
[10] J. Xu, N. J. Ghimire, J. S. Jiang, Z. L. Xiao, A. S. Botana, Y. L. Wang, Y. Hao, J. E. Pearson, and W. K. Kwok, Phys. Rev. B **96**, 075159 (2017).
[11] K. F. Wang, D. Graf, L. J. Li, L. M. Wang, and C. Petrovic, Sci. Rep. **4**, 7328 (2014).
[12] N. Kumar, Y. Sun, N. Xu, K. Manna, M. Y. Yao, V. Süss, I. Leermakers, O. Young, T. Förster, M. Schmidt, H. Borrmann, B. Yan, U. Zeitler, M. Shi, C. Felser, and C. Shekhar, Nat. Commun. **8**, 1642 (2017).
[13] M. Matin, R. Mondal, N. Barman, A. Thamizhavel, and S. K. Dhar, Phys. Rev. B **97**, 205130 (2018).
[14] R. Singha, A. Pariari, B. Satpati, and P. Mandal, Phys. Rev. B **96**, 245138 (2017).
[15] F. F. Tafti, Q. D. Gibson, S. K. Kushwaha, N. Haldolaarachchige, and R. J. Cava, Nat. Phys. **12**, 272 (2016).
[16] F. C. Chen, H. Y. Lv, X. Luo, W. J. Lu, Q. L. Pei, G. T. Lin, Y. Y. Han, X. B. Zhu, W. H. Song, and Y. P. Sun, Phys. Rev. B **94**, 235154 (2016).
[17] X. L. Wang, Y. Du, S. X. Dou, and C. Zhang, Phys. Rev. Lett. **108**, 266806 (2012).
[18] K. Shrestha, M. Chou, D. Graf, H. D. Yang, B. Lorenz, and C. W. Chu, Phys. Rev. B **95**, 195113 (2017).
[19] Z. K. Liu, J. Jiang, B. Zhou, Z. J. Wang, Y. Zhang, H. M. Weng, D. Prabhakaran, S-K. Mo, H. Peng, P. Dudin, T. Kim, M. Hoesch, Z. Fang, X. Dai, Z. X. Shen, D. L. Feng, Z. Hussain, and Y. L. Chen, Nat. Mater. **13**, 677 (2014).
[20] B. Q. Lv, N. Xu, H. M. Weng, J. Z. Ma, P. Richard, X. C. Huang, L. X. Zhao, G. F. Chen, C. E. Matt, F. Bisti, V. N. Strocov, J. Mesot, Z. Fang, X. Dai, T. Qian, M. Shi, and H. Ding, Nat. Phys. **11**, 724 (2015).
[21] S. Y. Xu, I. Belopolski1, N. Alidoust, M. Neupane, G. Bian, C. L. Zhang, R. Sankar, G. Q. Chang, Z. J. Yuan, C. C. Lee, S. M. Huang, H. Zheng, J. Ma, D. S. Sanchez, B. K. Wang, A. Bansil, F. C. Chou, P. P. Shibayev, H. Lin, S. Jia, and M. Z. Hasan, Science **349**, 613 (2015).

[22] Y. Wu, L. L. Wang, E. Mun, D. D. Johnson, D. X. Mou, L. Huang, Y. B. Lee, S. L. Bud'ko, P. C. Canfield, and A. Kaminski, Nat. Phys. **12**, 667 (2016).
[23] L. M. Schoop, M. N. Ali, C. Straßer, A. Topp, A. Varykhalov, D. Marchenko, V. Duppel, S. S. P. Parkin, B. V. Lotsch, and C. R. Ast, Nat. Commun. **7**, 11696 (2016).
[24] Y. P. Li, C. C. Xu, M. S. Shen, J. H. Wang, X. H. Yang, X. J. Yang, Z. W. Zhu, C. Cao, and Z. A. Xu, Phys. Rev. B **98**, 115145 (2018).
[25] P. Jensen, A. Kjekshus, and T. Skansen, Acta Chem. Scand. **20**, 403 (1966).
[26] B. Shen, X. Y. Deng, G. Kotliar, and N. Ni, Phys. Rev. B **93**, 195119 (2016).
[27] R. Singha, A. Kumar Pariari, B. Satpati, and P. Mandal, Proc. Natl. Acad. Sci. **114**, 2468 (2017).
[28] D. E Soule, Phys. Rev. **112**, 698 (1958).
[29] Z. W. Zhu, A. Collaudin, B. Fauqué, W. Kang, and K. Behnia, Nat. Phys. **8**, 89 (2011).
[30] See Supplemental Material at http://link.aps.org/supplemental/10.1103/PhysRevB.99.205116 for field-dependent MR with the magnetic field up to 14 T.
[31] L. X. Zhao, L. C. Xu, H. K. Zuo, X. M. Wu, G. Y. Gao, and Z. W. Zhu, Phys. Rev. B **98**, 085137 (2018).
[32] A. Narayanan, M. D. Watson, S. F. Blake, N. Bruyant, L. Drigo, Y. L. Chen, D. Prabhakaran, B. Yan, C. Felser, T. Kong, P. C. Canfield, and A. I. Coldea, Phys. Rev. Lett. **114**, 117201 (2015).
[33] R. Kealhofer, S. Jang, S. M. Griffin, C. John, K. A. Benavides, S. Doyle, T. Helm, P. J. W. Moll, J. B. Neaton, J. Y. Chan, J. D. Denlinger, and J. G. Analytis, Phys. Rev. B **97**, 045109 (2018).